Construction and Building Materials 220 (2019) 267–277

Contents lists available at ScienceDirect

Construction and Building Materials

journal homepage: www.elsevier.com/locate/conbuildmat

Deformation properties of silt solidified with a new SEU-2 binder

Shao-Yun Pu, Zhi-Duo Zhu *, Wei-Long Song, Hai-Rong Wang, Ren-Jie Wei

School of Transportation, Southeast University, Nanjing, Jiangsu Province 211189, China

HIGHLIGHTS

- SEU-2 binder improved the deformation properties and shear strength of silt.
- Stress-strain curves of SEU-2 binder solidified silt behaved as strain softening.
- Brittleness index increased with the increase of SEU-2 binder content.
- Silt structure became denser with the increase of SEU-2 content.
- Peak shear strength and residual strength with confining pressure increasing.

ARTICLE INFO

Article history:
Received 25 January 2019
Received in revised form 16 April 2019
Accepted 3 June 2019
Available online 10 June 2019

Keywords:
Silt
SEU-2 binder
Deformation
Shear strength
Brittleness index
Microscopic analysis

ABSTRACT

Solidification using binders is a widespread technique that provides civil engineering applications for silt with poor geotechnical performance. The aim of this study is to investigate the effects of a self-developed lab-made binder (named SEU-2 binder) on the deformation characteristics of silt. For this purpose, a series of one-dimensional consolidation tests, unconfined compressive tests, consolidated undrained triaxial compression tests, Scanning Electron Microscopy (SEM) tests and X-ray diffraction (XRD) tests were conducted on silt specimens and SEU-2 binder solidified silt specimens at 7, 28 and 90 days of curing. Brittleness index was introduced to evaluate the soft-hardening effect of solidified silt quantitatively. It was found that due to SEU-2 binder addition, the deformation characteristics of silt was improved. The initial void ratio and compression index decreased with the increase of SEU-2 binder content. Unconfined compressive strength (UCS) increased with curing time and SEU-2 binder content, while failure strain decreased. Moreover, the shear strength parameters of silt was enhanced due to SEU-2 binder addition, the cohesion increased with the increase of SEU-2 binder content, while the internal friction angle increased and then hardly changed. Additionally, under unconfined compressive tests, the stress-strain curves transformed from dwarf type to lanky type with SEU-2 binder dosage increasing. Under consolidated undrained triaxial compression tests, the stress-strain curves of SEU-2 binder solidified silt behaved as strain softening, while silt exhibited a strain hardening character under high confining pressure, exhibited a strain softening character under low confining pressure. The brittleness index increased with the increase of SEU-2 binder content. SEM analysis revealed that silt structure became denser with an increasing SEU-2 binder content. Furthermore, more network and fibrous hydrates such as C-S-H appeared with the increase of curing time.

1. Introduction

A silt is a fine-grained soil, or the fine-gained portion of a soil, with a plasticity index less than 4 or if the plot of plasticity index versus liquid limit falls below the 'A' line [1]. Silt has the characteristics of sandy soil and clayey soil. Silt with unsatisfactory grading consists of uniform fine-grained soil and its clay content such as montmorillonite and illite is very few. Moreover, silt has low plasticity index, loose, permeable and low cohesion properties and it is easy to hydrate when it is soaked, which determine the weak water cementation and poor anti-scouring performance of silt. The engineering characteristics of roadbed reclaimed with slit which is difficult to compact and easy to hydrate may store up hidden dangers for subgrade deformation, which creates bumps in the roadway and damage to the pavement [2,3]. Therefore, it must be treated to meet engineering requirements.

Solidification treatment is one of methods to improve mechanical properties of soil. Solidification not only improves the mechanical properties of soil, but also improves the compactibility

* Corresponding author.
E-mail address: zhuzhiduo@seu.edu.cn (Z.-D. Zhu).

https://doi.org/10.1016/j.conbuildmat.2019.06.016
0950-0618/

characteristics [4]. The method of using binder to treat soft soil has attracted widespread attention [5–8]. Many binders for soft soil have been developed and applied in engineering, such as slag [9,10], coal furnace fly ash [11,12], cement and lime [13], cement cellar kiln dust [14–16], domestic waste incineration slag [17], unconventional additives [18,19], lignin [20], alkaline activator [21–23], lime [24], etc. In practice, lime and water-hardening binder is widely used to treat soft soil [25–30]. Similarly, lime, cement, lime and cement mixtures are also widely used for silt solidification in engineering [13,31–34].

Because many binders are mainly developed for clay, but less for silt. In fact, silt roadbed and foundation are very common in engineering. Because silt is different from clay, if clay binder is directly used in silt, its applicability will be poor. Therefore, it is necessary to carry out research on silt binder. a new kind of binder (named SEU-2 binder) [35] was developed by Southeast University in 2006. The binder is composed of cement, admixture A (mineral powder and fly ash), CaO, expansive component A (alum, gypsum and Na_2SO_4), Surfactant B. The binder has high early strength, small shrinkage deformation, and high entire stiffness, adding 4% new stabilizing agent is an economic and reasonable method to solidify silt [36]. Additionally, the unconfined compressive strength, internal friction angle and cohesion of SEU-2 binder solidified silt are much larger than that of solidified silt with the same content of lime, cement and lime mixtures. In the past, the water stability and strength characteristics of SEU-2 binder was studied and the binder was applied to practical engineering [37]. However, as a kind of high-performance silt binder, not studies concerning its deformation characteristics could be found.

According to the published literature, it can be seen that although many achievements have been made in the research and development of silt binders, but not many studies have been done on SEU-2 binder for silt. Moreover, for SEU-2 binder, the existed studies concerning SEU-2 binder solidified silt generally focus on the influence of the content and curing time on the strength and water stability [36]. The deformation characteristics of solidified silt are very important for engineering, rare investigation has, however, been made to evaluate the deformation characteristics of silt solidified by incorporating SEU-2 binder. Therefore, the study on the deformation characteristics of SEU-2 binder solidified silt should be strengthened. Consequently, the aim of this paper is as follows: (a) investigating the deformation characteristics of SEU-2 binder solidified silt, (b) analyzing the effects of content and curing time on deformation characteristics, (c) analyzing some observations on the change in microstructure due to SEU-2 binder addition by using SEM, (d) analyzing reaction products in SEU-2 binder solidified silt by using XRD. The obtained research results provide some important references for the silt foundation treatment in engineering. However, such as this binder was developed specifically for silt and the applicability of this binder to clay or other types of soil will be the next research project.

2. Materials and testing program

2.1. Materials

2.1.1. Silt

The silt studied in this work was dredged from the waste Yellow River in Jiangsu province, China. ASTM D422-63 standard was used to determine particle size distribution. ASTM D4318-84 were used to determine the liquid and plasticity limits of silt. The X-ray fluorescence (XRF) method was used to determine the chemical compositions. Additionally, the XRD method was used to determine mineral compositions. The test results of basic physical characterization of silt at natural conditions are shown in Table 1. The main chemical compositions (shown in Table 2) are SiO_2 and Al_2O_3. Additionally, the mineral compositions were determined as shown in Table 3.

2.1.2. Binder

SEU-2 binder [35,36], a binder with high performance which was developed by Southeast University, is made of cement, admixture A, appropriate alkaline activating component, expansion component and surfactant. In this study, the binder was made by mixing and grinding the following components. Cement: Admixture A: CaO: Expansive component A: Surfactant B = 20: 48: 9.5: 22.5: 0.1. Additive A is a mixture of mineral powder and fly ash in a ratio of 1 to 1, Expansive component A is a mixture of alum, gypsum and sodium sulphate in a ratio of 6:2:1, Surfactant B is calcium sulfonate. Alkali activator is CaO powder. Before test, the SEU-2 binder by mixing the above components was prepared.

Table 1
Physical properties of silt.

Water content (%)	Density (g/cm^3)	Specific gravity	Void ratio	Liquid limit (%)[a]	Plastic limit (%)[a]	Particle size (mm) and content (%)[b]		
						2–0.074	0.074–0.002	<0.002
27.0	1.97	2.7	0.779	27.18	21.51	35.5	59.3	5.2

[a] Per ASTM D4318 (ASTM 2010).
[b] Measured using laser particle-size analyzer Mastersizer 2000.

Table 2
Chemical compositions of silt[a].

Composition	SiO_2	Al_2O_3	Fe_2O_3	TiO_2	CaO	MgO	K_2O	Na_2O	P_2O_3	SO_3	Loss on ignition	Organic matters
Content	74.64	10.20	6.53	0.54	0.63	0.74	1.44	0.57	0.078	0.027	0.52	4.10

[a] Measured by XRF spectrometer.

Table 3
Mineral compositions of silt.

Minerals	Content of non-clay minerals (%)							Content of non-clay minerals (%)				Other
	Total Content	Quartz	Mica	Feldspar	Calcite	White stone	Hornblende	Montmorillonite	Illite	Chlorite	kaolinite	
Content	65	40	8	7	7	3	Trace	10.2	5.6	5.2	4	10

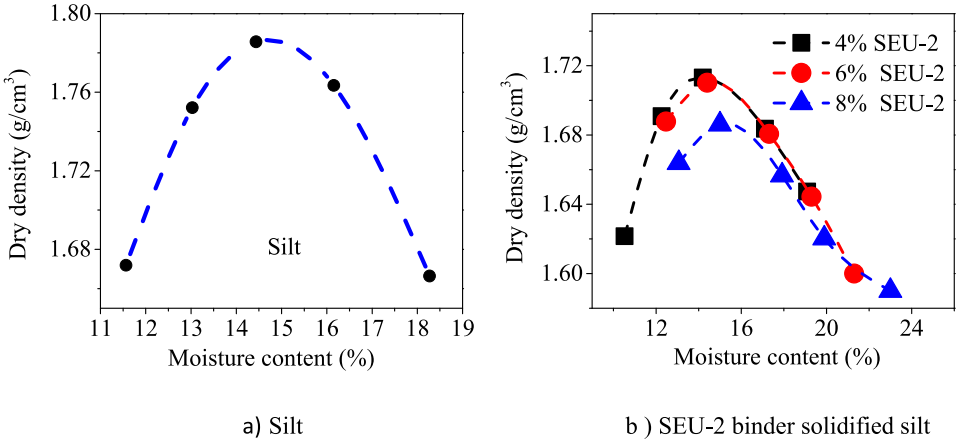

a) Silt b) SEU-2 binder solidified silt

Fig. 1. Compaction curves of silt and SEU-2 binder solidified silt.

Table 4
Compaction test results of SEU-2 binder solidified silt.

Binder	Content (%)	Optimum moisture content (%)	Maximum dry density (g/cm^3)
SEU-2	4	14.2	1.713
	6	14.4	1.710
	8	15.0	1.686

Moreover, all components were all dry during the preparation of the binder.

2.1.3. Compaction characteristics of silt and solidified silt

In this work, the distilled water was used as Feng's study [38]. The compaction test sample was a mixture of distilled water, SEU-2 binder and silt. Firstly, SEU-2 binder was mixed with silt evenly, and then distilled water was added. According to ASTM D698-12 [39], the standard proctor compaction tests were conducted on silt and SEU-2 binder solidified silt. The compaction curves obtained from the test are shown in Fig. 1. The maximum dry density of silt was 1.79 g/cm^3, and its optimum moisture content was 14.4%. The compaction test results of silt solidified by incorporating different contents of SEU-2 binder are shown in Table 4. From Table 4, as SEU-2 binder content increased, the optimum moisture content of SEU-2 binder solidified silt increased, while the maximum dry density decreased. A similar mechanical behavior can be found for lime solidified sediment, cement solidified sediment [40], volcanic ash, lime solidified clayey soil [41], cement solidified lateritic gravels [42]. The reason why the maximum dry density decreased with the increase of binder dosage is as follows. The addition of binders leads to an increasing affinity for water. Meanwhile, the added binders can wrap up fine soil particles to form large aggregates that occupy larger space [40–42]. Therefore, the optimum moisture content increased and the maximum dry density decreased with the increase of SEU-2 binder content.

2.2. Preparation of samples

Having obtained the compaction results, the air-dried silt was thoroughly mixed with 4%, 6% and 8% SEU-2 binder, respectively. Specifically, a certain amount of binder was mixed with air-dried silt evenly, then a certain amount of distilled water was added into the mixtures according to the optimum moisture content in Table 4 and stirring it well until it was well-distributed. After 24 h of enclosing material, the prepared mixtures were put into the different sample makers and compacted. After compaction, for unconfined compression tests, the specimens were shaped in cylindrical mold with 5 cm inner diameter and 10 cm height, sealed in polyethylene plastic bags, and then stored in humidity chamber of constant temperature (20 ± 3 °C) for 7, 28 and 90 days, respectively until tested. For triaxial compression tests, the specimens were shaped in cylindrical mold with 3.91 cm inner diameter and 8 cm height and stored in curing chamber of constant temperature (20 ± 3 °C) for 28 days. For one-dimensional consolidation tests, after compaction, the specimen was shaped in cutting ring with 6.18 cm diameter and 2 cm height, then stored in curing chamber of constant temperature (20 ± 3 °C) for 28 days.

2.3. Testing programs

For the purposes of this study, a series of one-dimensional consolidation tests, unconfined compressive tests and consolidated undrained triaxial compression tests were performanced on silt and SEU-2 binder solidified silt specimens under standard curing. Moreover, SEM and XRD tests were also conducted. The specific process for the test is as follows:

2.3.1. Unconfined compressive tests

The unconfined compressive tests was carried out by YSH-2 type unconfined compressive gauge. A series of unconfined compressive tests were carried out on the specimens at 7, 28 and 90 days of curing, according to, Chinese test methods of soils for highway engineering (JTG E40-2007) [43], Chinese test methods materials stabilized with inorganic binder materials for highway engineering (JTJ E51-2009) [44], ASTM D4219 [45]. The vertical compression rate was fixed at 1%/min until samples failed. Each unconfined compressive test was conducted in triplicate.

2.3.2. Triaxial consolidated-undrained (CU) triaxial tests

The consolidated-undrained (CU) triaxial experiments were carried out by TSZ-2 full-automatic triaxial apparatus producted by Zhilong technology Co., Ltd. in Nanjing city, Jiangsu province, China. A series of consolidated-undrained triaxial tests were carried out on the specimens at 28 days of curing after it were soaked under water at the last day of each curing period according to Chinese test methods of soils for highway engineering (JTG E40-2007) [43] and ASTM D2850 [46]. The vacuum saturation method was used to saturate these specimens, and the loading rate was fixed at 0.24 mm/min until samples failed. The applied confining pressure was was 100, 200 and 300 kPa.

2.3.3. One-dimensional consolidation tests

The one-dimensional consolidation tests was carried out by WG consolidation apparatus. The one-dimensional consolidation tests were conducted on silt and SEU-2 binder solidified silt specimens at 28 days of curing according to Chinese test methods of soils for highway engineering (JTG E40-2007) [43] and ASTM D2435 [47]. Axial loading classifications were 25, 50, 100, 200, 400, 800 kPa.

2.3.4. Scanning Electron Microscope (SEM) and X-ray diffraction (XRD) tests

Scanning Electron Microscope (SEM) technique is widely used in the analysis of micro-structure and micro-material of soils [48–52]. According to the requirements of SEM test, firstly silt and SEU-2 binder solidified silt at 28 days of curing were cut, then these prepared samples were put into drying oven to be vacuum drying for 24 h. Finally thedried samples were placed in the spraying apparatus to spray a thin layer of conductive material. After that, these samples were coated with gold film and then tested by SEM. The Scanning Electron Microscopy S-3000N used for testing was produced by Hitachi Company of Japan.

3. Results and discussion

3.1. One-dimensional consolidation tests

Fig. 2 shows the compression curves of silt and solidified silt for 28 days of curing. Silt and SEU-2 binder solidified silt show different compression characteristics in one-dimensional consolidation tests. As can be seen from Fig. 2a, the initial void ratio of solidified silt was smaller than that of silt, and it decreased with the increase of SEU-2 binder content. As Bergado's [53] and C.F. Chiu's [54] study, for cement solidified soft clay, the void ratio of cement solidified soft clay also decreases with the increase of cement binder content. The reason for the decrease in void ratio is due to the functions of volume expansion and filling up voids of binder. Or / and because a series of physical and chemical reactions happen between binder and mineral compositions in silt, thus producing some hydrates which cements silt particles and fills up macropores between silt particles.

In Fig. 2a, when the vertical load was 0–25 kPa, the compression deformation of silt was not much different from that of silts solidified by incorporating different contents of SEU-2 binder. When silt and solidified silt were subjected to a smaller load, the compression deformation of the specimen was mainly caused by the decrease of the pore volume of silt, and the deformation is primarily elastic deformation. When the load exceeded 25 kPa, the deformation of silt was much larger than that of SEU-2 binder solidified silt. The main reason for this is that the structure of silt was destroyed rapidly under a larger load, thus the curve gradient in compression curves of silt was larger than that of SEU-2 binder solidified silt.

Table 5
Consolidation test results.

Parameters	Silt	4% SEU-2 binder	6% SEU-2 binder	8% SEU-2 binder
Compression coefficient (MPa^{-1})	0.30	0.13	0.11	0.08
Constrained elastic modulus (MPa)	6.45	13.99	16.95	20.83

It can also be seen from Fig. 2a that there was a turn point in compression curves of silt, the stress at the turn point is the yield stress, which reflects the compressive properties of soil. There are two ways to determine the yield stress of solidified soil. The yield stress can be determined from e-logp curves proposed by Casagrande and ln (1 + e)–logp proposed by Butterfield [55]. Obviously, the yield stress of silt was 25 kPa from e-logp curves shown in Fig. 2a. Unfortunately, because the maximum measuring range of WG consolidation apparatus is 800 kPa in the consolidation tests, the yield stress of SEU-2 binder solidified silt can not be determined from e-1ogp curves and the ln (1 + e)–logp shown in Fig. 2. However, these problems could be solved if a consolidation apparatus with a wider range measure is used in subsequent studies.

Table 5 presents coefficient of compression index and constrained elastic modulus. From Table 5, it is observed that the coefficient of compression index decreased with an increase in SEU-2 binder content. it suggested the effect of SEU-2 binder on silt is very obvious, the compressibility of silt can be reduced due to the addition of SEU-2 binder.

3.2. Unconfined compressive tests

Each unconfined compressive test was conducted in triplicate, the abnormal test data was deleted. The stress –strain curves of silt solidified with different contents of SEU-2 binder at 7, 28 and 90 days are shown in Fig. 3. Several parameters such as failure strain ε_f and unconfined compressive strength (UCS) can be obtained from the full stress–strain curves. It can be seen from Fig. 3 that the initial portion (low strain stage) of the stress–strain curves can be considered as a straight line, so the stress was proportional to strain with the constant of proportionality. As the strain increased, the stress continued to rise until the peak stress in accordance with a nonlinear law. The peak stress is called as unconfined compressive strength and and the strain at peak strength is considered as failure strain ε_f [56].

It can be seen from Fig. 3 that the stress-strain curves of SEU-2 binder solidified silt exhibited softening character. Furthermore,

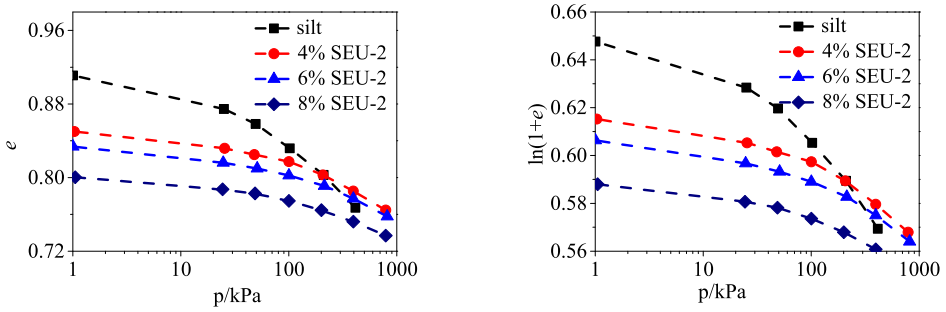

a). e-logp curves of silt and solidified silt b). ln(1+e)-logp curves of silt and solidified silt

Fig. 2. Silt and solidified silt compression curves.

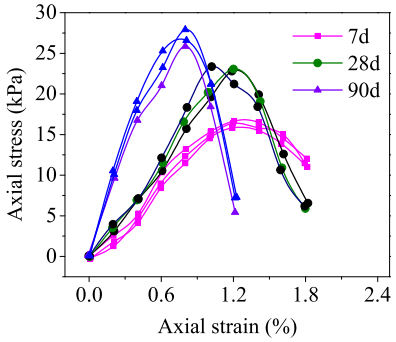

a). Uniaxial stress-strain curve of 4% SEU-2 binder

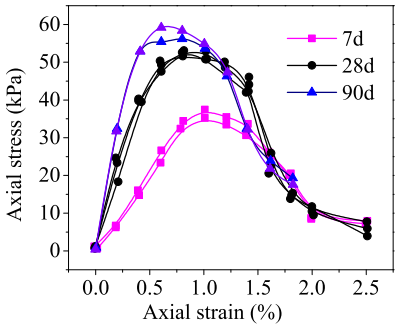

b). Uniaxial stress-strain curve of 6% SEU-2 binder

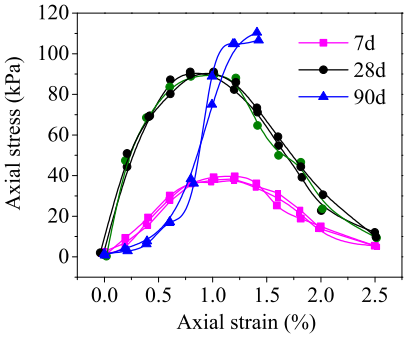

c). Uniaxial stress-strain curve of 8% SEU-2 binder

Fig. 3. Stress-strain curves of silt solidified with different SEU-2 bider content.

the SEU-2 binder content had somehow influence on the shape of the stress-strain curves, the stress-strain curves transformed from dwarf type to lanky type with SEU-2 binder dosage increasing. However, at 90 days of curing, the stress-strain curves of 8% SEU-2 binder solidified silt were different from that of 4% and 6% SEU-2 binder solidified silt.

For 8% SEU-2 binder solidified silt, when the strain did not reach 0.6%, the stress increased very slowly with the strain increasing, after the strain exceeded 0.6%, a sudden increase in stress. After reaching the peak stress, the specimen immediately disintegrated and showed obvious brittle failure. The tangential modulus of 8% SEU-2 binder solidified silt at 7 and 28 days of curing approached a fixed value. Furthermore, the tangential modulus of silt solidified with 8% SEU-2 binder showed increase in modulus from 7 to 28 days of curing. However, at 90 days of curing, the initial tangential modulus had a sudden decrease, then as the strain increased, tangential modulus increased. Obviously, the stress-strain characteristics of solidified silt changed. which indicated that when the SEU-2 binder content and curing time increase to a certain value, the content and curing time may influence the stress-strain characteristic of solidified silt. The reason for this phenomenon may be as follows: As the curing time and SEU-2 binder content increased, more hydrates were formed by the reaction of binder with mineral components in silt, the hydrates can wrap up fine soil particles to form large aggregates that occupy larger space, as well as fill pore. The compaction characteristics of formed hydrates may determine this mechanical properties. Further research is needed on this phenomenon.

3.2.1. Stress–strain relationships of solidified silt at different curing times

From Fig. 3, the effect of curing time on ε_f and UCS shown in Fig. 4 can be obtained. As can be seen from Fig. 4a and b, in general, failure strain ε_f decreased with an increase in curing time, while UCS increased. Taking 6% SEU-2 binder solidified silt as an example, the peak stresses at 7, 28 and 90 days of curing were 380.22 kPa, 558.02 kPa and 611.72 kPa, respectively. The corresponding failure strains ε_f were 1%, 0.8% and 0.7%, respectively.

3.2.2. Stress–strain curves of silt solidified by various contents of SEU-2 binder

Fig. 5 presents the effect of SEU-2 binder content on UCS and ε_f. It can be clearly observed from Fig. 5 that the UCS increased with the increase of SEU-2 binder content, while the failure strain ε_f decreased, except 8% SEU-2 binder solidified silt at 90 days of curing.

3.3. Triaxial compression testscompressive test (CU)

3.3.1. Triaxial stress-strain characteristics of solidified silt

To study the influence of confining pressure on the deformation characteristics of solidified silt, the consolidated-undrained (CU) triaxial shear tests results of silt and solidified silt at 28 days of curing are plotted in Fig. 6. Fig. 6 shows the effect of confining pressure on the deviatoric stress-strain curves of untreated silt and silt solidified with 4%, 6% and 8% SEU-2 binder. In Fig. 6, σ_1 is the maximum principal stress, σ_3 is minimum principal stress.

In Fig. 6, it is possible to observe important differences in the deformation characteristics of these untreated and solidified specimens. it can be observed from Fig. 6 that the stress-strain curves of SEU-2 binder solidified silt behaved as strain softening, while silt exhibited a strain hardening character under high confining pressure, exhibited a strain softening character under low confining pressure. Silt presented a nonlinear stress-strain curves before the peak stress. However, solidified silt presented a approximate linear stress-strain curves. Additionally, compared with untreated silt, solidified silt had a more obvious softening effect.

It can be seen from Fig. 6 that the deviational stress $(\sigma_1 - \sigma_3)$ increased and then decreased with the increase of axis strain ε_1. After reaching a maximum deviatoric stress $(\sigma_1 - \sigma_3)_f$, the deviatoric stress $(\sigma_1 - \sigma_3)$ rapidly declined until a residual stress was

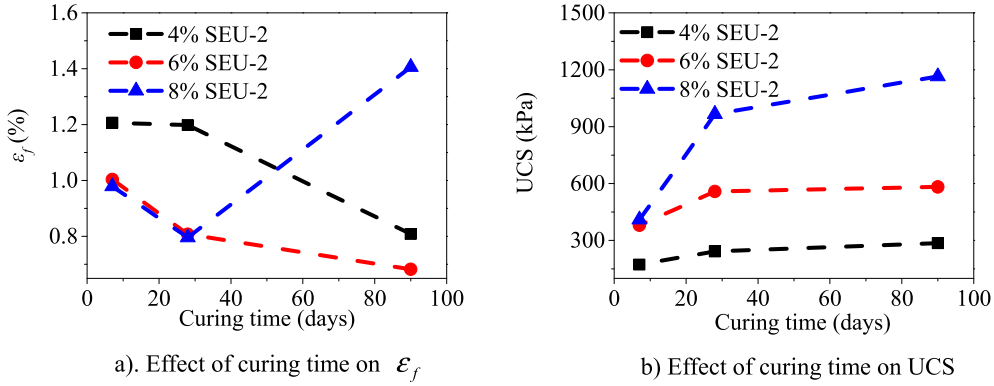

a). Effect of curing time on ε_f b) Effect of curing time on UCS

Fig. 4. Effect of curing time on ε_f and UCS.

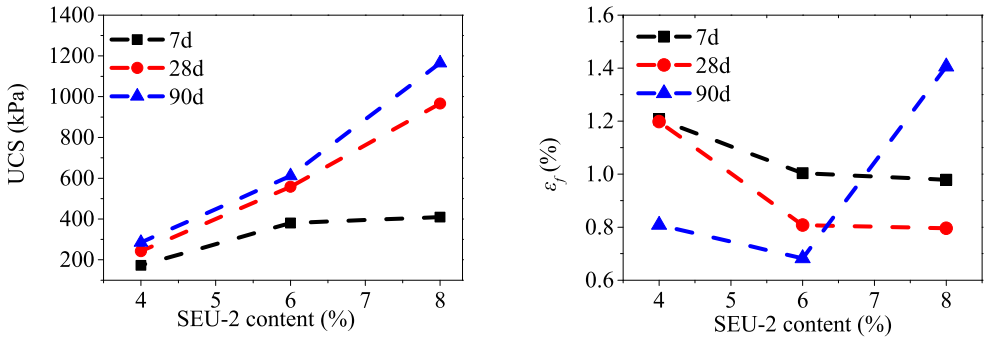

a). Effect of SEU-2 binder content on UCS **b)**. Effect of SEU-2 binder content on ε_f

Fig. 5. Effect of SEU-2 binder content on UCS and ε_f.

reached which was approximately a fixed value considered as residual strength $(\sigma_1 - \sigma_3)_r$. Additionally, the confining pressure had little effect on the initial modulus of SEU-2 binder solidified silt, but has an obvious effect on peak shear strength and residual strength. Specifically, the peak strength increased with the increase of confining pressure. In this paper, when axial strain ε_1 reached 0.2, the corresponding deviational stress was defined as the residual strength. Moreover, the residual strength increased with confining pressure.

From Fig. 6b, the peak deviatoric stress increased from 5.670 kPa to 9.695 kPa when the confining pressure increased from 100 to 300 kPa for 4% SEU-2 binder solidified silt. Due to the increase of confining pressure, the increase of normal stress acting on shear surface which in turn increased the resisting shear component along the shear plane [57]. The peak deviatoric stress for 100 kPa confining pressure appeared at an axial strain of 3.51% and for 300 kPa confining pressure it was 4.405% with a percentage increase of 25%.

Fig. 6c presents the deviatoric stress-axial strain curves of 6% SEU-2 binder solidified silt. From Fig. 6c, the peak deviatoric stress increased from 9.912 kPa to 13.216 kPa when the confining pressure increased from 100 to 300 kPa . The peak deviatoric stress for 100 kPa confining pressure appeared at an axial strain of 3.21% and for 300 kPa confining pressure it was 3.914% with a percentage increase of 21.93% .

Fig. 6d presents the deviatoric stress-axial strain relationship of 8% SEU-2 binder solidified silt, the peak deviatoric stress increased from 13.124 kPa to 17.496 kPa when the confining pressure increased from 100 to 300 kPa. The peak deviatoric stress for 100 kPa confining pressure appeared at an axial strain of 2.277% and for 300 kPa confining pressure it was3.651% with a percentage increase of 60.34%.

Taking 4%, 6% and 8% SEU-2 binder solidified silts under 200 kPa confining pressure example. The peak deviatoric stress increased from 8.378 kPa to 15.509 kPa when the binder content increased from 4% to 8%. The peak deviatoric stress for 4% SEU-2 binder occurred at an axial strain of 4.427% and for 8% SEU-2 binder, it was 2.291% with a percentage decrease of 48.24%.

Under the same confining pressure, as the SEU-2 binder content increased, the peak shear strength and residual strength increased, while axial failure strain ε_{1f} decreased. The result suggested the brittleness increased with the increased dosage of SEU-2 binder. Under the same dosage of SEU-2 binder, the peak strength, axis failure strain ε_{1f} and residual strength increased with an increase in confining pressure.

3.3.2. Variation of shear strength parameters

Shear strength parameters from consolidated-undrained (CU) triaxial tests of silt and solidified silt are shown in Fig. 7. In Fig. 7, the effects of SEU-2 binder contents on internal friction angle ϕ and cohesion c can be observed. As the SEU-2 binder content increased, the cohesion c increased (*vide* Fig. 7b), while internal friction angle ϕ increased and then hardly changed (*vide* Fig. 7a). Furthermore, the cohesion c and internal friction angle ϕ increased in a nonlinear law. Obviously, the addition of SEU-2 binder can improve the shear strength of silt. The increase of shear strength parameters c and ϕ can be attributed to the increased

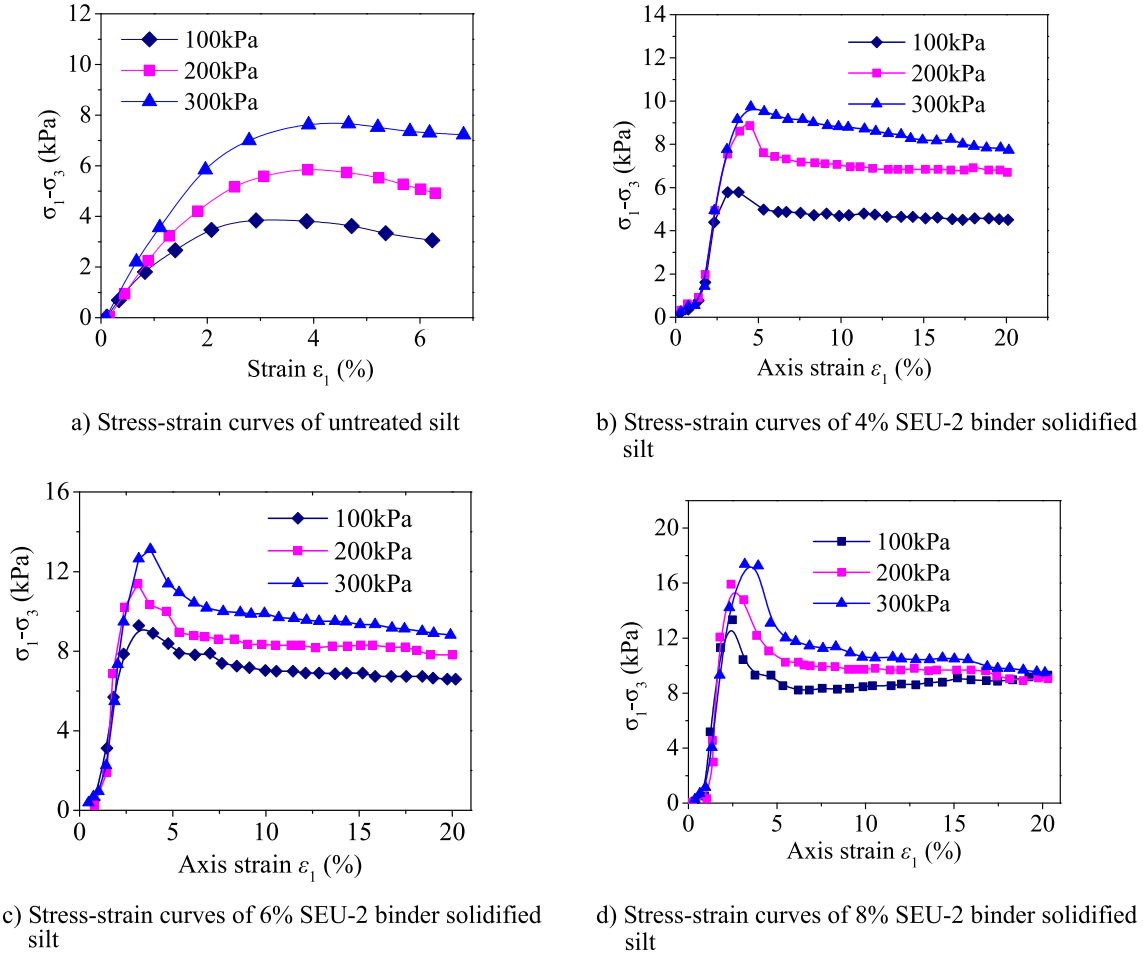

a) Stress-strain curves of untreated silt

b) Stress-strain curves of 4% SEU-2 binder solidified silt

c) Stress-strain curves of 6% SEU-2 binder solidified silt

d) Stress-strain curves of 8% SEU-2 binder solidified silt

Fig. 6. Stress-strain curves of different contents of SEU-2 binder solidified silt.

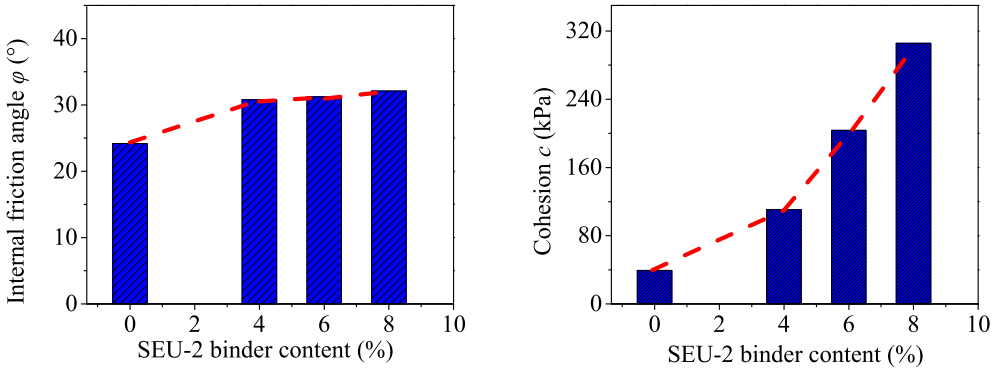

a) Effect of content on Internal friction angle φ

b) Effect of content on cohesion c

Fig. 7. Effect of content on shear strength parameters.

contact area between the silt particles due to the presence of SEU-2 binder. Additionally, a series of gels were formed by the reaction of SEU-2 binder and the silicon and aluminum substances in silt, the gels can improve shear strength parameters [36].

3.3.3. Variation of brittleness index

Brittleness index (I_B) is not only a material parameter but also a deformation parameter. Brittleness index can be used to reflect the strain softening extent of soil. The larger the I_B, the greater its brittleness. Brittleness index I_B proposed by Bishop [58] is defined as the ratio of the difference value of the maximum and minimum deviatoric stress to the maximum deviatoric stress. The expression of I_B is as follows.

$$I_B = \frac{(\sigma_1 - \sigma_3)_f - (\sigma_1 - \sigma_3)_r}{(\sigma_1 - \sigma_3)_f} \quad (1)$$

Obviously, the larger I_B, the greater soil brittleness. When $I_B = 0$, the brittleness disappears completely and the soil is in a ideal plastic state. When $I_B = 1$, soil is liquefied completely. Based on

Table 6
Parameters of shear strength of stabilized silt.

Binder	Strength parameters	Confining pressure (kPa)		
		100	200	300
4% SEU-2	$(\sigma_1-\sigma_3)_f$ (kPa)	572.5	880.5	972.4
	$(\sigma_1-\sigma_3)_r$(kPa)	445.2	667.2	784.3
	I_B	0.222	0.242	0.193
6% SEU-2	$(\sigma_1-\sigma_3)_f$(kPa)	937	1157	1367.4
	$(\sigma_1-\sigma_3)_r$(kPa)	654	770.6	874.5
	I_B	0.302	0.334	0.36
8% SEU-2	$(\sigma_1-\sigma_3)_f$(kPa)	1315	1650	1763
	$(\sigma_1-\sigma_3)_r$(kPa)	820	903	965
	I_B	0.376	0.426	0.453

parameter $I_B$defined above, the test results of SEU-2 binder solidified silt are arranged in Table 6. It can be clearly seen from Table 6 that there was an increase in $I_B$with the increase of SEU-2 binder content, indicating that the brittleness increases with the increase of SEU-2 binder content (*vide* Fig. 8). However, there was also an increase in $I_B$of 4% and 6% SEU-2 binder solidified silt with the confining pressure increasing, the I_B of 4% SEU-2 binder solidified silt increased and then decreased (*vide* Fig. 9). Therefore, the relationship between confining pressure and brittleness index can not be determined from this study.

3.4. Microscopic analysis of silt and SEU-2 binder solidified silt

Four different specimens at 7 and 28 days of standard curing including untreated, 4%, 6% and 8% SEU-2 binder solidified ones were subjected to XRD and SEM analysis. The microstructural analysis can help to analyze the curing mechanism, deformation and strength development of solidified silt due to the addition of SEU-2 binder.

The microstructures of different contents of SEU-2 binder solidified silts at 7 and 28 days of curing and untreated silt at the magnification 300 × 300 are shown in Fig. 10. It is observed from these micrographs that there were many differences between untreated silt and solidified silt. The SEU-2 binder solidification can be seen to have strongly modified the original silt texture at the micrometer scale. For untreated silt, it is clearly observed from Fig. 10a that silt had a very loose structure, there were a certain number of irregular particles and some large macropores between particles. Additionally, there was almost no amorphous substance between particles. After adding SEU-2 binder, fine silt particles were cemented into a larger aggregate, and the characteristic of structural instability was improved. Meanwhile, the void was filled with binder, so these solidified silt specimens had a denser structure (*vide* Fig. 10). Furthermore, the uniformity, compactness of specimens and wholeness of aggregates got better and these aggregates became larger with the increase of SEU-2 binder. These facts show that SEU-2 binder can improve the deformation and shear strength significantly.

The principle of SEU-2 solidification was cementation and bonding, cohesion. When the silt was mixed with SEU-2 binder, these cementitious hydrates such as C-S-H produced by the reaction between SEU-2 binder and compositions in silt not only strengthen the cementation between silt particles, but also fill up the voids, thus improving destruction-resisting ability and deformation of silt, as well as increasing its cohesion and internal friction angle. Consequently, the shear strength increased accordingly with the increase of dosage of SEU-2 binder.

In order to study the effect of curing time on micro-mechanism, and analyze the formed cementitious hydrates in SEU-2 binder solidified silt. The microstructures of 8% SEU-2 binder solidified silt

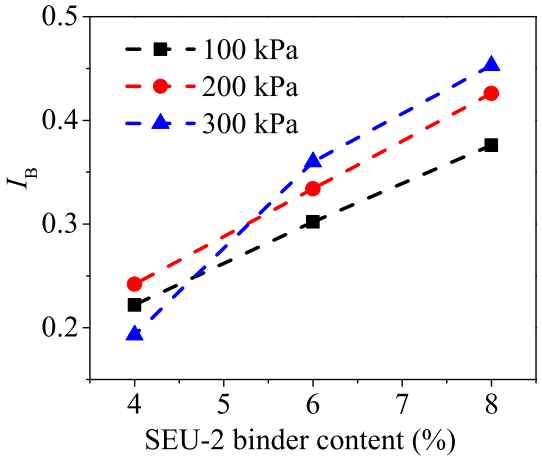

Fig. 8. Effect of SEU-2 binder content on I_B.

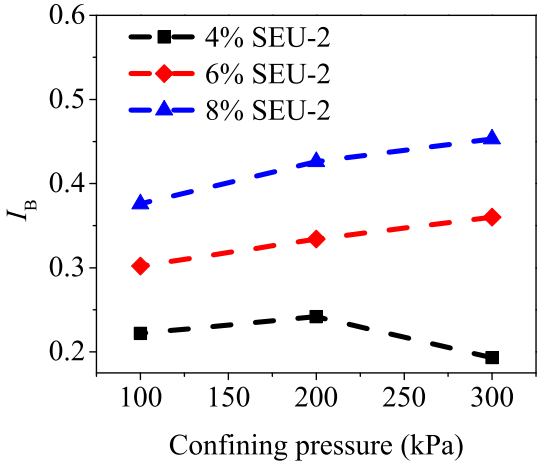

Fig. 9. Effect of confining pressure on I_B.

at 7 and 28 days of curing at the magnification 5000 × 5000 shown in Fig. 11 are selected for this study. It can be seen form Fig. 11 that at 7 days of curing, some short columnar aggregates appeared, silt particles was cemented loosely. At 28 days of curing, a large number of network and fibrous gels appeared. Additionally, a large amount of needle-like hydrates appeared. With the increase of curing time, more hydrates appeared, so the strength increased. The fibrous gels are C-S-H as previous research [36]. These cementious hydrates were further determined by XRD diagram shown in Fig. 12.

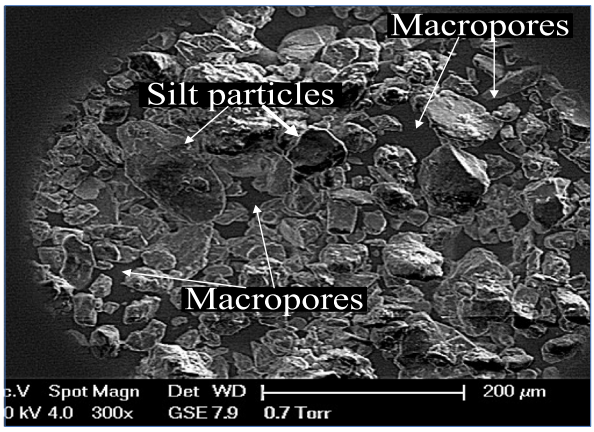

a) Silt

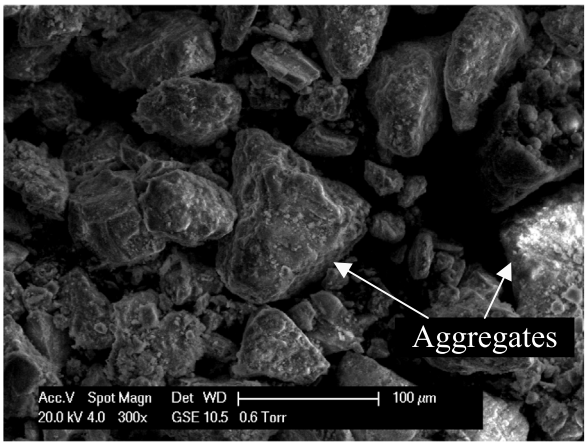

b) 4% SEU-2 binder solidified silt

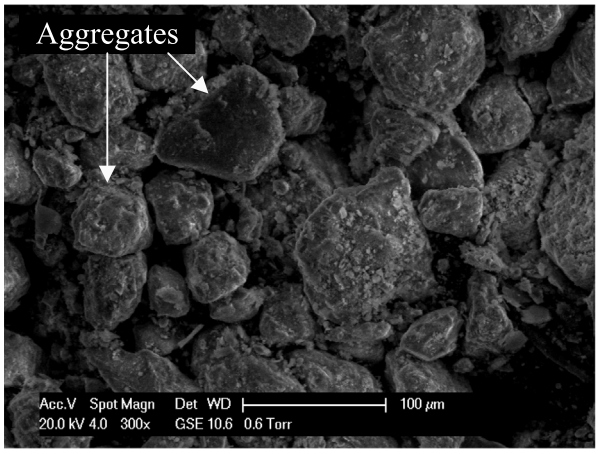

c) 6% SEU-2 solidified silt

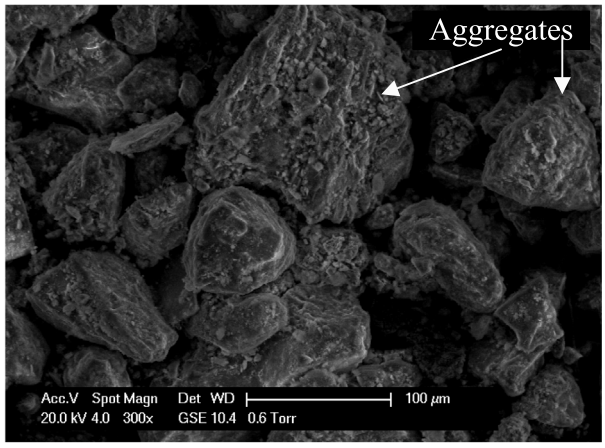

d) 8 % SEU-2 binder solidfied silt

Fig. 10. SEM pictures of silt by incorporating different contents of SEU-2 binder at 28 days of curing.

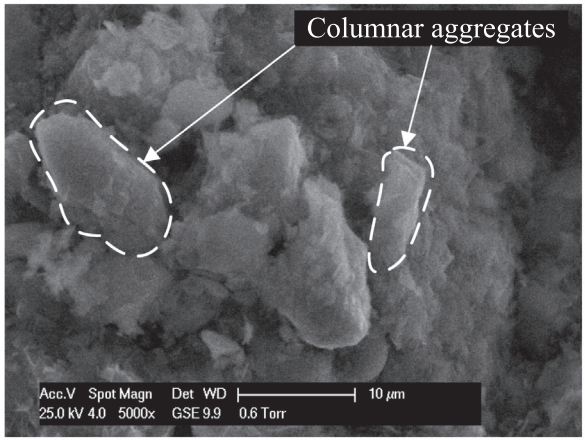

a). 8% SEU-2 binder solidified binder silt at 7 days of curing

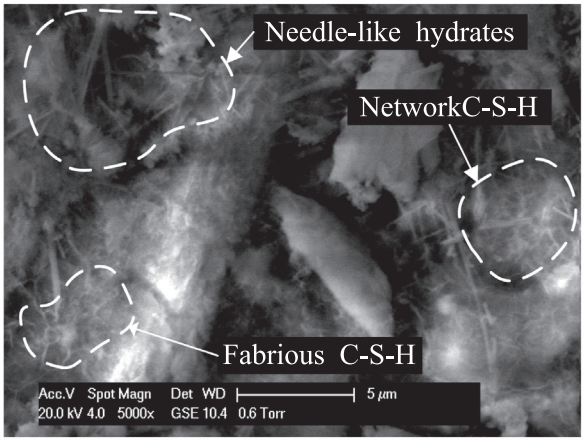

b). 8% SEU-2 binder solidified silt at 28 days of curing

Fig. 11. SEM pictures of silt by incorporating different contents of SEU-2 binder.

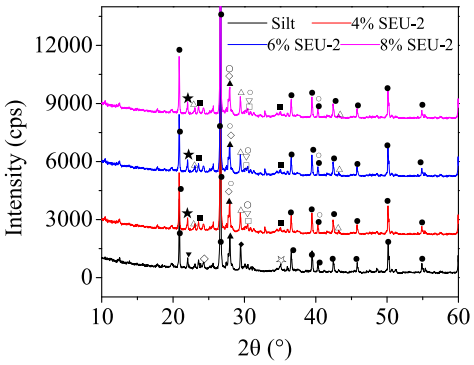

Fig. 12. XRD diagram of silt and SEU-2 binder solidified silt at 7 days of curing. ● Quartz: SiO_2 △ Calcite: $CaCO_3$ □ Mordenite-[Ca]: $CaAlSi_{10024}{\cdot}7H_2O$ ☆ Kaolinite ▲ Bayerite: $Al(OH)_3$ ◇ Unnamed zeolite: $CaO{\cdot}Al_2{\cdot}zSiO_2{\cdot}xH_2O$ ■ Margarite-2 M1: $CaAl_2Si_2Al_2O_{10}OH_2$ ★Albite low: $Na[AlSi_3O_8]$ ◆ Cordierite: $Mg_2Al_4Si_5O_{18}$ ▼ Crystobalite low: SiO_2 ▽Calcium Silicate hydrate: $Ca_2SiO_4{\cdot}0.35H_2O$ ○ Calcium silicate aluminum hydrate: $Ca_8Al_{16}Si_{24080}{\cdot}18.9H_2O$.

Fig. 12 is the XRD diagram of unreated silt and SEU-2 binder solidified silt at 7 days of curing. It can be seen that the silt compositions were basically consistent with the results in Table 3. For silt solidified by different contents of SEU-2 binder, the shape and variation of peaks in the XRD were basically same. Compared with the XRD diagram of untreated silt, some new peaks of low strength appeared due to the addition of SEU-2 binder, indicating that some new hydrates such as Calcium Silicate hydrate $Ca_2SiO_4{\cdot}0.35H_2O$ (C-S-H) and Calcium silicate aluminum hydrate $Ca_8Al_{16}Si_{24080}{\cdot}18.9H_2O$ (C-S-A-H) were formed. Meanwhile, Calcite $CaCO_3$ was also found. The detected Calcium Silicate hydrate $Ca_2SiO_4{\cdot}0.35H_2O$ may be fibrous C-S-H mentioned above. The formed compounds were the source of strength-given components of SEU-2 binder solidified silt, and can improve the mechanical properties of silt. Consequently, SEU-2 binder can improve the strength and deformation characteristics of silt.

4. Conclusions

This paper analyzes deformation characteristics of SEU-2 binder solidified silt by one-dimensional consolidation tests, unconfined compressive tests, consolidated undrained triaxial compression tests, SEM tests and XRD tests. The following conclusions can be drawn from this study.

(1) Due to the addition of SEU-2 binder, the compressibility of silt decreased. Namely, the initial void ratio and the compression coefficient of silt decreased with the increase of SEU-2 binder content.
(2) Under unconfined compression tests, the stress-strain curves of SEU-2 binder solidified silt transformed from dwarf type to lanky type with an increasing SEU-2 binder dosage. With the increase of curing time and SEU-2 binder content, failure strain decreased, while UCS increased.
(3) The stress-strain curves of SEU-2 binder solidified silt behaved as strain softening. However, silt exhibited a strain hardening characteristics under high confining pressure, exhibited a strain softening characteristics under low confining pressure.
(4) The internal friction angle ϕ of silt increased and then hardly changed with the increase of SEU-2 binder content, while the cohesion c increased.
(5) Under consolidated-undrained (CU) triaxial shear tests, the axis failure strain of SEU-2 binder solidified silt decreased with the increase of curing time, while peak deviatoric stress increased. Additionally, as SEU-2 binder dosage increased, the peak deviatoric stress and the brittleness index of SEU-2 binder solidified silt increased, while the axis failure strain decreased.
(6) Silt structure became denser with the increase of SEU-2 binder content. Furthermore, more compounds appeared with the increase of curing time.

Declaration of Interest

The authors declared that there is no conflict of interest.

Acknowledgments

The authors express their deep gratitude to Dr. Wei Duan for their help during the research. We are also grateful to the Construction and Building Materials editor and reviewers for their constructive suggestion and kind help in improving the quality of the manuscript. The authors acknowledge financial support from the National Natural Science Fund (no. 40872173).

References

[1] ASTM, D2487, Standard practice for classification of soils for engineering purposes (unified soil classification system)., in: ASTM International West Conshohocken, PA, 2011
[2] A.J. Puppala, N. Intharasombat, R.K. Vempati, Experimental studies on ettringite-induced heaving in soils, J. Geotech. Geoenviron. Eng. 131 (2005) 325–337.
[3] G.J. Cai, S.Y. Liu, L.Y. Tong, Field evaluation of deformation characteristics of a lacustrine clay deposit using seismic piezocone tests, Eng. Geol. 116 (2010) 251–260.
[4] C. Tang, B. Shi, G. Wei, F.J. Chen, Y. Cai, Strength and mechanical behavior of short polypropylene fiber reinforced and cement stabilized clayey soil, Geotext. Geomembr. 25 (3) (2007) 194–202.
[5] D. Little, Stabilization of Pavement Subgrade and Base Courses with Lime, Kendall/Hunt Publishing Compagny, Dubuque, Iowa, USA, 1995, p. 219.
[6] N. Cabane, Sols traités à la chaux et aux liants hydrauliques: Contribution à l'identification et à l'analyse des éléments perturbateurs de la stabilisation PhD thesis, Ecole Supérieure Nationale des Mines de Saint-Etienne, France, 2006.
[7] B.R. De, Etude des sols traités à la chaux, à l'échelle microscopique et à l'échelle macroscopique DEA thesis, Université Libre de Bruxelles, 2006.
[8] B.R. De, Q. Bollens, C.A. Gomes, P.H. Duvignaud, J.C. Verbrugge, Time and temperature dependency of the geomechanical properties of silty soils treated with lime, in: Proc. Int. Conf. on Advance Characterization of Pavment and Soil Materials, Taylor & Francis/Balkema, Athènes, 2007, pp. 513–521.
[9] H.Y. Poh, G.S. Ghataora, N. Ghazireh, Soil stabilization using basic oxygen steel fine slags, J. Mater. Civ. Eng. 18 (2) (2006) 229–240.
[10] S. Wild, J.M. Kinuthia, G.I. Jones, D.D. Higgins, Effects of partial substitution of lime with ground granulated blast furnace slag (GGBS) on strength properties of lime-stabilized sulphate-bearing clay soils, Eng. Geol. 51 (1) (1998) 37–53.
[11] S. Kolias, V. Kasselouri-Rigopoulou, A. Karahalios, Stabilisation of clayey soils with high calcium fly ash and cement, Cem. Concr. Compos. 27 (2) (2005) 301–313.
[12] K.Y. Show, J.H. Tay, A.T.C. Goh, Reuse of incinerator fly ash in soft soil stabilization, J. Mater. Civ. Eng. 15 (4) (2003) 335–343.
[13] K. Lemaire, D. Deneele, S. Bonnet, M. Legret, Effects of LC mixtures treatment on the physicochemical, microstructural and mechanical characteristics of a plastic silt, Eng. Geol. 166 (2013) 255–261.
[14] Z.A. Baghdadi, M.N. Fatani, N.A. Sabban, Soil modification by cement kiln dust, J. Mater. Civ. Eng. 4 (1997) 218–222.
[15] G.A. Miller, S. Azad, Influence of soil type on stabilization with cement kiln dust, Constr. Build. Mater. 14 (2) (2000) 89–97.
[16] D.J. Rivard-Lentz, L.R. Sweeney, K.R. Demars, Incinerator Bottom ash as a Soil Substitute: Physical and Chemical Behaviour 1275, ASTM Sp Techn Publ, 1997, pp. 246–262.
[17] H. Kukko, Stabilization of clay with inorganic by-products, J. Mater. Civ. Eng. 12 (4) (2000) 307–309.
[18] A. Seco, F. Ramirez, L. Miqueleiz, B. Garcia, E. Prieto, The use of nonconventional additives in Marls stabilization, Appl. Clay Sci. 51 (2011) 419–423.
[19] C. Urena, J.M. Azanon, F. Corpas, F. Nieto, C. Leon, L. Perez, Magnesium hydroxide, seawater and olive mill wastewater to reduce swelling potential and plasticity of bentonite soil, Constr. Build. Mater. 45 (2013) 289–297.
[20] G. Cai, T. Zhang, S. Liu, et al., Stabilization Mechanism and effect evaluation of stabilized silt with lignin based on laboratory data, Mar. Georesour. Geotechnol. 34 (4) (2016) 331–340.
[21] M. Zhang, H. Guo, T. El-Korchi, G. Zhang, M. Tao, Experimental feasibility study of geopolymer as the next-generation soil stabilizer, Constr. Build. Mater. 47 (2013) 1468–1478.

[22] N. Cristelo, S. Glendinning, L. Fernandes, A.T. Pinto, Effect of calcium content on soil stabilisation with alkaline activation, Constr. Build. Mater. 29 (2012) 167–174.
[23] L. Verdolotti, S. Iannace, M. Lavrogna, R. Lamanna, Geo-polymerization reaction to consolidate incoherent pozzolanic soil, J. Mater. Sci. 43 (3) (2007) 865–873.
[24] D.N. Little, Stabilization of pavement subgrades and base courses with lime, Base course (1995).
[25] D. Osula, Lime modification of problem laterite, Eng. Geol. 30 (2) (2016) 141–154.
[26] F.G. Bell, Lime stabilization of clay minerals and soils, Eng. Geol. 42 (4) (1996) 223–237.
[27] S. Wild, J.M. Kinuthia, G.I. Jones, D.D. Higgins, Effects of partial substitution of lime with ground granulated blast furnace slag (GGBS) on the strength properties of lime-stabilised sulphate-bearing clay soils, Eng. Geol. 51 (1) (1998) 37–53.
[28] O. Cuisinier, J.C. Auriol, T.L. Borgne, D. Deneele, Microstructure and hydraulic conductivity of a compacted lime-treated soil, Eng. Geol. 123 (3) (2011) 187–193.
[29] O. Cuisinier, D. Deneele, F. Masrouri, Shear strength behaviour of compacted clayey soils percolated with an alkaline solution, Eng. Geol. 108 (3–4) (2009) 177–188.
[30] F. Sariosseiri, B. Muhunthan, Effect of cement treatment on geotechnical properties of some Washington State soils, Eng. Geol. 104 (1–2) (2009) 119–125.
[31] G. Russo, S.D. Vecchio, G. Mascolo, Microstructure of a lime stabilised compacted silt, in: Experimental Unsaturated Soil Mechanics, Springer Proceedings in Physics, 2009, pp. 49–56.
[32] L.B. Runigo, O. Cuisinier, Y.J. Cui, D. Deneele, Impact of initial state on the fabric and permeability of a lime-treated silt under long-term leaching, Can. Geotech. J. 46 (2009) 1243–1257.
[33] R. Jauberthie, F. Rendell, D. Rangeard, L. Molez, Stabilisation of estuarine silt with lime and/or cement, Appl. Clay Sci. 50 (3) (2010).
[34] X.Z. Yuan, S.D. Li, W. Cui, Silt Subgrade Modification and Stabilization with Ground Granulated Blast Furnace Slag and Carbide Lime in Areas with a Recurring High Groundwater, International Conference on Mechanic Automation & Control Engineering, IEEE, 2010.
[35] C.X. Qian, S.Y. Liu. Soil stabilizer, Chinese patent, CN 1730836,(2006).
[36] Z.D. Zhu, S.Y. Liu, Utilization of a new soil stabilizer for silt subgrade, Eng. Geol. 97 (3) (2008) 192–198.
[37] Z.D. Zhu, Study on stabilization of silt subgrade: theory and application, Ph.D. Dissertation for Southeast University, 2006. in Chinese.
[38] Y.S. Feng, Y.J. Du, K.R. Reddy, W.Y. Xia, Performance of two novel binders to stabilize field soil with zinc and chloride: mechanical properties, leachability and mechanisms assessment, Constr. Build. Mater. 189 (2018) 1191–1199.
[39] ASTM. 2012. Standard test methods for laboratory compaction characteristics of soil using standard effort (12 400 ft-lbf/ft3 (600 kN-m/m3). ASTM standard D698-12. American Society for Testing and Material, West Conshohocken, Pa
[40] D.X. Wang, N.E. Abriak, R. Zentar, W.Y. Xu, Solidification/stabilization of dredged marine sediments for road construction, Environ. Technol. 33 (2012) 95–101.
[41] K.M.A. Hossain, M. Lachemi, S. Easa, Stabilized soils for construction applications incorporating natural resources of Papua New Guinea, Resour. Conserv. Recycl. 51 (2007) 711–731.
[42] Y. Millogo, M. Hajjaji, R. Ouedraogo, M. Gomina, Cement-lateritic gravels mixtures: Microstructure and strength characteristics, Constr. Build. Mater. 22 (2008) 2078–2086.
[43] Ministry of Communications of the People's Republic of China. Test methods of soils for Highway engineering. China communication press, Beijing. 2007.
[44] Ministry of Communications of the People's Republic of China. Test methods materials stabilized with inorganic binder materials for highway engineering. China communication press, Beijing, 2009.
[45] ASTM. 2008, Standard test method for unconfined compressive strength index of chemical- grouted soils. ASTM standard D4219-08. American Society for testing and Materials, West Conshohocken, Pa
[46] ASTM D2850-15, Standard Test Method for Consolidated Undrained Triaxial Compression Test for Cohesive Soils; ASTM International: West Conshohocken, PA, USA, 2015.
[47] ASTM D2435/D2435M-11, Standard Test Methods for One-Dimensional Consolidation Properties of Soils Using Incremental Loading.
[48] J.S. Tchalenko, The microstructure of London clay, J. Engrg. Geol. I (1968) 155–168.
[49] W.D. Keller, The nascence of clay minerals, Clays Clay Miner. 33 (1985) 161–172.
[50] S. Diamond, J.L. White, W.L. Dolch, Transformation of Clay Minerals by Calcium Hydroxide Attack, in: Proc. 12th Nat. Con on Clays and Clay Minerals, Pergamon Press, New York, N.Y, 1985, pp. 359–379.
[51] J.B. Croft, The structure of soils stabilized with cementitious agents, J. Engrg. Geol. 2 (1985) 63–80.
[52] S.N. Rao, G. Rajasekaran, Reaction products formed in lime-stabilized marine Clays, J. Geotech. Eng. 122 (5) (1996) 329–336.
[53] D.T. Bergado, C. Taechakumthorn, G.A. Lorenzo, H.M. Abuel-Naga, Stress deformation behavior under anisotropic drained triaxial consolidation of cementtreated soft Bangkok clay, Soils Found. 46 (5) (2006) 629–637.
[54] C.F. Chiu, W. Zhu, C.L. Zhang, Yielding and shear behaviour of cement-treated dreged materials, Eng. Geol. 103 (2008) 1–12.
[55] R. Butterfield, A natural compression law for soils, Geotechinique 29 (4) (1979) 469–480.
[56] D.X. Wang, N.E. Abriak, R. Zenta, Strength and deformation properties of Dunkirk marine sediments solidified with cement, lime and fly ash, Eng. Geol. 166 (2013) 90–99.
[57] G.L.S. Babu, M.E.R. Jaladurgam, Strength and deformation characteristics of fly ash mixed with randomly distributed plastic waste, J. Mater. Civ. Eng. 26 (12) (2014) 04014093.
[58] A.W. Bishop, Progressive failure–with special reference to the mechanism causing it // Proceedings of the Geotechnical Conference, Norway: Oslo, (1967) 142-150